IET Microwaves, Antennas & Propagation

Research Article

Filtering rat-race couplers with impedance transforming characteristics based on terminated coupled line structures

ISSN 1751-8725
Received on 20th September 2019
Revised 20th December 2019
Accepted on 3rd March 2020
E-First on 27th April 2020
doi: 10.1049/iet-map.2019.0631
www.ietdl.org

Gaoya Dong[1], Weimin Wang[1], Yongle Wu[1] ✉, Yuanan Liu[1], Manos M. Tentzeris[2]
[1]*Beijing Key Laboratory of Work Safety Intelligent Monitoring, School of Electronic Engineering, Beijing University of Posts and Telecommunications, P.O. Box 282, 100876, People's Republic of China*
[2]*School of Electrical Computer Engineering, Georgia Institute of Technology, Atlanta, Georgia, 30332, USA*
✉ *E-mail: wuyongle138@gmail.com*

Abstract: In this study, a series of rat-race couplers with bandpass filtering responses and impedance transforming characteristics are presented based on novel coupled-line structures. Firstly, a novel filtering rat-race coupler core circuit is proposed by introducing coupled-line structures into conventional rat-race coupler. Then, a series of rat-race couplers with enhanced filtering responses and stopband rejections are constructed by employing various types of impedance transformers. The even- and odd-mode methods are adopted to explain the operating mechanisms. Finally, a filtering rat-race coupler prototype with a fractional bandwidth of 35.2% is designed and measured. The measured results show high passband selectivity, good out-of-band rejection and isolation performances, which is attractive for practical application.

1 Introduction

Rat-race coupler is an important passive component that can divide/combine radio frequency signals with a phase difference of 180° in various circuits such as balanced mixer, balanced amplifier as well as antenna feeding structure. However, the operating bandwidth (BW) of the conventional rat-race coupler is quite narrow, which makes it unsuitable for a wideband communication system. Some efforts have been done to extend the operating BW of rat-race coupler. In [1, 2], the finite-ground-plane coplanar waveguide is adopted to design wideband rat-race couplers. In [3, 4], branch-line couplers with wide passband is presented by utilising multi-sectional branch lines. A hybrid branch-line coupler for wideband and space-limited applications is designed in [5] by cascaded slow-wave cells in place of conventional transmission lines (TLs). Broadband rat-race couplers have been proposed in [6, 7] by utilising a tight-coupled-line section.

In practical application, the rat-race coupler is often cascaded with a bandpass filter to select wanted signals and suppress unwanted signals. Some couplers integrated with filtering responses or wide out-of-band rejection suppression performances have been proposed in [8–16], which have the advantages of compact size and reduced insertion loss. A novel narrow-band filtering rat-race coupler (FRC) is reported in [8] by employing a dual-mode cross-shaped dielectric resonator. Based on substrate-integrated waveguide, a rat-race coupler with passband selectivity is presented in [9]. Rat-race couplers with filtering responses are presented in [10, 11] by utilising coupled resonators. In [12], a compact FRC implemented in low-temperature co-fired ceramic technology is presented based on the eight-line spatially-symmetrical coupled structure.

In addition to wide passband BW and high filtering response, good harmonic suppression and wide upper stopband rejection performances are demanded to suppress the out-of-band interferences, i.e. background noise and intermodulation signals from non-linear components. In [13], a coupled-resonator network is introduced to design a rat-race coupler with passband selectivity and upper stopband rejection performance. A compact rat-race coupler with high passband selectivity and good out-of-band rejection is proposed in [14] by employing dual-mode stub-loaded resonators. In [15], four $\pm K$-inverters with bandpass functions are utilised to replace the one- or three-quarter-wavelength TLs in the conventional rat-race coupler, and a FRC with wide out-of-band rejection is realised in [15]. A novel compact FRC with good out-of-band rejection is implemented in [16] by adopting 2×2 cross coupled configuration based on hairpin resonators. However, the BW of the rat-race couplers designed in [13–16] all is <13%.

In this study, a novel method of designing wideband compact FRC with wide and deep out-of-band rejection performance is presented. The core circuit of FRC is designed by replacing $\lambda/4$ TL in a conventional rat-race coupler with coupled-lines (CLs) and various impedance transformers (ITs) are loaded into core circuit to realise improved impedance matching and enhanced out-of-band rejection performances. The operating mechanisms of the presented FRC are detailed explained based on the even- and odd-mode method. To validate the proposed idea, a FRC with a fractional BW (FBW) of 35.2% is fabricated and measured.

2 General construction of the proposed coupler

The circuit topology of a conventional rat-race coupler (180° hybrid) is shown in Fig. 1*a*, which consists of three sections of $\lambda/4$ TLs and one $3\lambda/4$ TL, all with the characteristic impedance of $\sqrt{2}Z_0$. The signals input from port 1 can be equally distributed into ports 2 and 3 with the same phase, while port 4 is isolated. If the signals are excited from port 4, they will be equally divided into ports 2 and 3 with a phase difference of 180°, and port 1 is isolated.

By replacing the $\lambda/4$ TLs in the conventional rat-race coupler with parallel CLs, the schematic of the presented FRC core circuit (FRCC) is obtained and exhibited in Fig. 1*b*. Moreover, the proposed FRCC is composed of three parallel CLs $((Z_{1e},\ Z_{1o}, \theta)$, $(Z_{1e},\ Z_{1o}, \theta)$, and $(Z_{2e},\ Z_{2o}, \theta))$ and one $3\lambda/4$ TL $(\sqrt{2}Z_0,\ 3\theta)$. Define $(Z_{ne} + Z_{no})/2 = Z_{na}$, $(Z_{ne} - Z_{no})/2 = Z_{nb}$, $Z_{cn} = \sqrt{Z_{ne}Z_{no}}$ $(n \in 1, 2, 3)$ and $k_n = Z_{nb}/Z_{na}$. The phase velocities of microstrip CLs in even- and odd-mode are assumed equal. The electrical lengths (θ) are all selected as 90° at centre frequency (f_0), and the characteristic impedance in ports 1, 2, 3, and 4 are all selected as 50 Ω. Then various ITs are employed to construct the designed FRC whole circuit (FRWC), and the schematic of FRWC is shown in Fig. 1*c*. Moreover, the filtering performances and impedance matching characteristics are greatly improved in FRWC by adopting various ITs.

According to Ang and Leong [17], the rat-race coupler can be considered conceptually as the combination of an in-phase power divider and an out-of-phase power divider. To realise equal in-

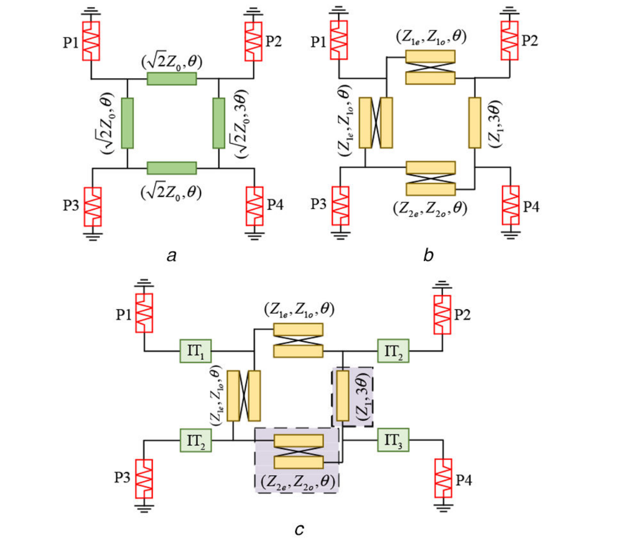

Fig. 1 *Schematics of*
(a) Conventional rat-race coupler, ***(b)*** Proposed FRCC, ***(c)*** Proposed FRWC

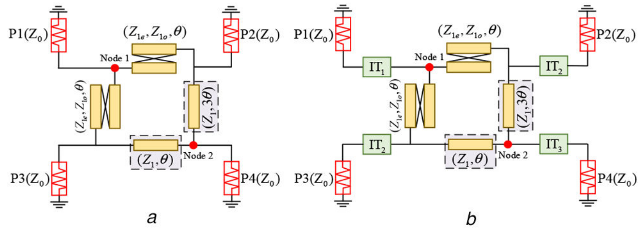

Fig. 2 *Simplified schematics of proposed*
(a) FRCC, ***(b)*** FRWC

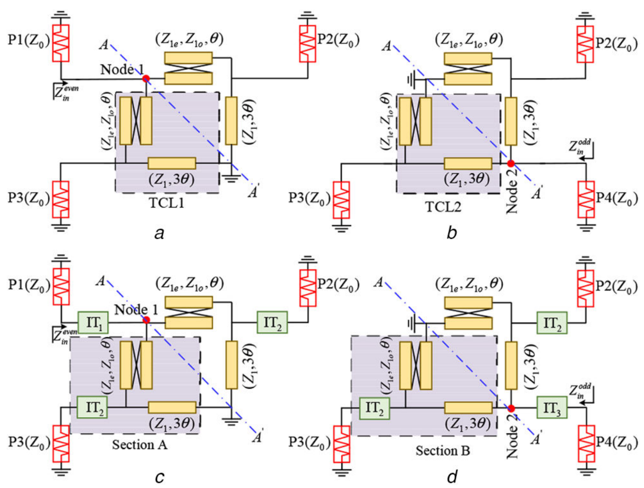

Fig. 3 *The even- and odd-mode equivalent circuit*
(a) Even-mode equivalent circuit of the proposed FRCC, ***(b)*** Odd-mode equivalent circuit of the proposed FRCC, ***(c)*** Even-mode equivalent circuit of the proposed FRWC, ***(d)*** Odd-mode equivalent circuit of the proposed FRWC

phase power divider between ports 1, 2, 3 and equal out-of-phase power divider between ports 4, 2, and 3, the transmission characteristics of CLs and TL in shaded areas shown in Fig. 1*c* should be equivalent to each other. The related analyses of CLs and TL are carried out. Based on the TL theory and four-port impedance matrix of CLs demonstrated in [18], the input impedances of specific TL and CLs could be deduced as

$$Z_{\text{in}}^{\text{TL}} = Z_1\frac{Z_{\text{T}} + \text{j}Z_1\tan 3\theta}{Z_1 + \text{j}Z_{\text{T}}\tan 3\theta} \tag{1a}$$

$$Z_{\text{in}}^{\text{CL}} = \frac{Z_{2a}Z_{\text{T}}\sin\theta\cos\theta + \text{j}(Z_{2b}^2 - Z_{2a}^2\cos^2\theta)}{Z_{2a}\sin\theta\cos\theta + \text{j}Z_{\text{T}}\sin^2\theta} \tag{1b}$$

When $Z_{\text{in}}^{\text{TL}} = Z_{\text{in}}^{\text{CL}}$ is satisfied with arbitrary Z_{T}, the transmission characteristics of TL and CLs could be considered as equivalent. The expressions of $Z_{\text{in}}^{\text{TL}}$ ($Z_{\text{in}}^{\text{CL}}$) could be simplified as Z_1^2/Z_{T} (Z_{2b}^2/Z_{T}) based on (1) at f_0. Thus, the transmission characteristics of TL and CLs could be considered as equivalent to each other when $Z_{2b} = Z_1$. Based on the above analysis, when $Z_{2b} = Z_1$ is fulfilled, the schematic of FRCC and FRWC could be simplified as Fig. 2 by replacing the specific CLs with TL.

Based on the simplified schematic of FRWC shown in Fig. 2, under even-mode excitation at ports 2 and 3, the signals arrive at node 1 with equal magnitude and phase to obtain the sum signals at port 1, while these signals reach node 2 with equal magnitude and opposite phase to realise isolation at port 4. Under odd-mode signals excitation at ports 2 and 3, the signals arrive at node 1 with equal magnitude and opposite phase to provide isolation at port 1, while these signals reach node 2 with equal magnitude and phase to obtain the sum signals at port 4. Owing to $\tan\theta = \tan(\pi + \theta)$, the values of $\tan\theta$ and $\tan 3\theta$ are equal to each other at f_0 when the electrical lengths (θ) are all selected as 90° at f_0. To simplify analysis, the TL (Z_1,θ) can be replaced by TL $(Z_1, 3\theta)$ at f_0. Thus, the even- and odd-mode equivalent circuits of presented FRCC and FRWC are depicted in Fig. 3.

3 Operating principles of FRCC

To explain the in-phase power splitting performance between ports 1, 2, and 3, the simplified even-mode equivalent circuit of FRCC is analysed in the following. Based on [18], the ***ABCD*** matrix of coupled lines can be expressed as

$$\begin{pmatrix} \boldsymbol{A}_C & \boldsymbol{B}_C \\ \boldsymbol{C}_C & \boldsymbol{D}_C \end{pmatrix} = \begin{pmatrix} \dfrac{Z_a}{Z_b}\cos\theta & \text{j}\dfrac{Z_b^2\csc^2\theta - Z_a^2\cot^2\theta}{Z_b\csc\theta} \\ \text{j}\dfrac{1}{Z_b\csc\theta} & \dfrac{Z_a}{Z_b}\cos\theta \end{pmatrix} \tag{2}$$

where $Z_a = (Z_e + Z_o)/2$, $Z_b = (Z_e - Z_o)/2$. Then the ***ABCD*** matrix of TCL1 exhibited in Fig. 3*a* can be deduced as

$$\begin{pmatrix} \boldsymbol{A}_{\text{TCL1}} & \boldsymbol{B}_{\text{TCL1}} \\ \boldsymbol{C}_{\text{TCL1}} & \boldsymbol{D}_{\text{TCL1}} \end{pmatrix} = \begin{pmatrix} \dfrac{Z_a}{Z_b}\cos\theta + \dfrac{Z_b^2\csc^2\theta - Z_a^2\cot^2\theta}{Z_1 Z_b\tan 3\theta\csc\theta} & \text{j}\dfrac{Z_b^2\csc^2\theta - Z_a^2\cot^2\theta}{Z_b\csc\theta} \\ \text{j}\dfrac{1}{Z_b\csc\theta} - \text{j}\dfrac{Z_a}{Z_1 Z_b\tan 3\theta}\cos\theta & \dfrac{Z_a}{Z_b}\cos\theta \end{pmatrix} \tag{3}$$

Under even mode excitation, the ***ABCD*** matrix between port 1 and port 2 can be extracted as

$$\begin{pmatrix} \boldsymbol{A}_{12} & \boldsymbol{B}_{12} \\ \boldsymbol{C}_{12} & \boldsymbol{D}_{12} \end{pmatrix} = \begin{pmatrix} \boldsymbol{A}_{\text{TCL1}} & \boldsymbol{B}_{\text{TCL1}}/2 \\ 2\boldsymbol{C}_{\text{TCL1}} & \boldsymbol{D}_{\text{TCL1}} \end{pmatrix} \tag{4}$$

Thus, the input impedance in port 1 ($Z_{\text{in}}^{\text{even}}$) can be expressed as

$$Z_{\text{in}}^{\text{even}} = \frac{\boldsymbol{A}_{12}Z_0/2 + \boldsymbol{B}_{12}}{\boldsymbol{C}_{12}Z_0/2 + \boldsymbol{D}_{12}} \tag{5}$$

Moreover, port 4 is isolated under even-mode excitation, the reflection coefficient (S_{11}) and transmission coefficient (S_{21}, S_{31}) can be deduced as

$$|S_{11}| = \left|\frac{Z_{\text{in}}^{\text{even}} - Z_0}{Z_{\text{in}}^{\text{even}} + Z_0}\right| \tag{6a}$$

$$|S_{21}| = |S_{31}| = \left|\frac{\sqrt{2Z_{\text{in}}^{\text{even}}Z_0}}{Z_{\text{in}}^{\text{even}} + Z_0}\right| \tag{6b}$$

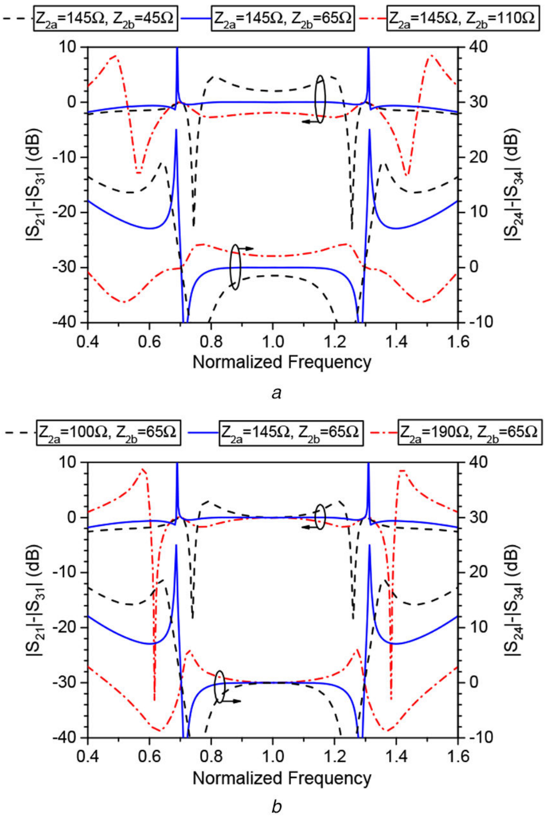

Fig. 4 *Amplitude differences with various*
(a) Z_{2b}, ***(b)*** Z_{2a}

By substituting (2)–(5) into (6a), the return loss in port 1 (S_{11}) could be expressed as (7a). In a specific case, the expression of S_{11} can be simplified as (7b) at f_0

$$|S_{11}| = \left| \frac{2\boldsymbol{C}_{\mathrm{TCL1}} Z_0^2 + (2\boldsymbol{D}_{\mathrm{TCL1}} - \boldsymbol{A}_{\mathrm{TCL1}}) Z_0 - \boldsymbol{B}_{\mathrm{TCL1}}}{2\boldsymbol{C}_{\mathrm{TCL1}} Z_0^2 + (2\boldsymbol{D}_{\mathrm{TCL1}} + \boldsymbol{A}_{\mathrm{TCL1}}) Z_0 + \boldsymbol{B}_{\mathrm{TCL1}}} \right| \tag{7a}$$

$$|S_{11}| = \left| \frac{2Z_0^2 - \dfrac{k_1^2}{1-k_1^2} Z_{c1}^2}{\dfrac{k_1^2}{1-k_1^2} Z_{c1}^2 + 2Z_0^2} \right| \tag{7b}$$

Transmission zeros (TZs) in the in-phase operation can be obtained when $|S_{11}| = 1$. Below $2f_0$, the frequencies of TZs can be calculated as (8a) and (8b) based on (2)–(6)

$$f_{\mathrm{TZ1}}^{\mathrm{even}} = \frac{2f_0}{3} \tag{8a}$$

$$f_{\mathrm{TZ2}}^{\mathrm{even}} = \frac{4f_0}{3} \tag{8b}$$

To illustrate the out-phase power splitting characteristics in ports 4, 2 and 3, the simplified odd-mode equivalent circuit of FRCC is analysed as following. Based on the TL theory and four-port impedance matrix of CLs demonstrated in [18], the ***ABCD*** matrix of TCL2 could be calculated as

$$\begin{pmatrix} \boldsymbol{A}_{\mathrm{TCL2}} & \boldsymbol{B}_{\mathrm{TCL2}} \\ \boldsymbol{C}_{\mathrm{TCL2}} & \boldsymbol{D}_{\mathrm{TCL2}} \end{pmatrix} = \begin{pmatrix} \cos 3\theta + \dfrac{Z_a Z_1 \sin 3\theta \cot\theta}{Z_b^2 \csc^2\theta - Z_a^2 \cot^2\theta} & jZ_1 \sin 3\theta \\ j\sin 3\theta / Z_1 + \mathrm{j}\dfrac{Z_a \cot\theta \cos 3\theta}{Z_a^2 \cot^2\theta - Z_b^2 \csc^2\theta} & \cos 3\theta \end{pmatrix} \tag{9}$$

The matrix between ports 4 and 2 can be deduced as

$$\begin{pmatrix} \boldsymbol{A}_{42} & \boldsymbol{B}_{42} \\ \boldsymbol{C}_{42} & \boldsymbol{D}_{42} \end{pmatrix} = \begin{pmatrix} \boldsymbol{A}_{\mathrm{TCL2}} & \boldsymbol{B}_{\mathrm{TCL2}}/2 \\ 2\boldsymbol{C}_{\mathrm{TCL2}} & \boldsymbol{D}_{\mathrm{TCL2}} \end{pmatrix} \tag{10}$$

Thus, the input impedance ($Z_{\mathrm{in}}^{\mathrm{odd}}$) in port 4 could be specifically expressed as

$$Z_{\mathrm{in}}^{\mathrm{odd}} = \frac{\boldsymbol{A}_{42} Z_0/2 + \boldsymbol{B}_{42}}{\boldsymbol{C}_{42} Z_0/2 + \boldsymbol{D}_{42}} \tag{11}$$

The reflection coefficient (S_{44}) and transmission coefficient (S_{24}, S_{34}) can be calculated as

$$|S_{44}| = \left| \frac{Z_{\mathrm{in}}^{\mathrm{odd}} - Z_0}{Z_{\mathrm{in}}^{\mathrm{odd}} + Z_0} \right| \tag{12a}$$

$$|S_{24}| = |S_{34}| = \left| \frac{\sqrt{2 Z_{\mathrm{in}}^{\mathrm{odd}} Z_0}}{Z_{\mathrm{in}}^{\mathrm{odd}} + Z_0} \right| \tag{12b}$$

because port 1 is isolated under odd-mode excitation. The return loss in port 4 (S_{44}) can be expressed as (13a) by taking (9–11) into (12a). In a specific case, at f_0, the expression of S_{44} can be simplified as (13b)

$$|S_{44}| = \left| \frac{2\boldsymbol{C}_{\mathrm{TCL2}} Z_0^2 + (2\boldsymbol{D}_{\mathrm{TCL2}} - \boldsymbol{A}_{\mathrm{TCL2}}) Z_0 - \boldsymbol{B}_{\mathrm{TCL2}}}{2\boldsymbol{C}_{\mathrm{TCL2}} Z_0^2 + (2\boldsymbol{D}_{\mathrm{TCL2}} + \boldsymbol{A}_{\mathrm{TCL2}}) Z_0 + \boldsymbol{B}_{\mathrm{TCL2}}} \right| \tag{13a}$$

$$|S_{44}| = \left| \frac{2Z_0^2 - Z_1^2}{2Z_0^2 + Z_1^2} \right| \tag{13b}$$

TZs in the out-of-phase operation can be obtained when $|S_{44}| = 1$. Below $2f_0$, the frequencies of TZs can be calculated as (14a) and (14b) based on (9)–(13)

$$f_{\mathrm{TZ1}}^{\mathrm{odd}} = \frac{2f_0}{\pi} \arccos\left(\frac{Z_{1b}}{Z_{1a}}\right) = \frac{2f_0}{\pi} \arccos(k_1) \tag{14a}$$

$$f_{\mathrm{TZ2}}^{\mathrm{odd}} = 2f_0 - \frac{2f_0}{\pi} \arccos\left(\frac{Z_{1b}}{Z_{1a}}\right) = 2f_0 - \frac{2f_0}{\pi} \arccos(k_1) \tag{14b}$$

Based on Fig. 4*a*, when Z_1 is selected as 65 Ω, the amplitude differences ($|S_{21}| - |S_{31}|$) and ($|S_{24}| - |S_{34}|$) during passband can be tuned by changing the value of Z_{2b}. Moreover, $Z_{2b} = Z_1$ should be satisfied to realise equal power splitting at f_0, which accords to the analysis demonstrated in Section 2. Amplitude imbalances across the passband can be adjusted by changing the value of Z_{2a}, as depicted in Fig. 4*b*. Consequently, the optimised amplitude differences and imbalances across the whole passband range could be achieved by choosing the appropriate values of Z_{2b} and Z_{2a}, respectively.

To further explain the adjustment mechanisms of passband BW and in-band return loss, the frequency responses with various parameters are investigated. From Fig. 5*a*, under even-mode excitation, the constant passband BW and various in-band return losses could be realised with different values of k_1, which has a good agreement with (7b). As observed from Fig. 5*b*, under odd-mode excitation, constant in-band return losses level and various passband BWs are obtained with different values of k_1. Moreover, the frequencies adjustment mechanisms of TZs ($f_{\mathrm{TZ1}}^{\mathrm{even}}$, $f_{\mathrm{TZ2}}^{\mathrm{even}}$, $f_{\mathrm{TZ1}}^{\mathrm{odd}}$, and $f_{\mathrm{TZ2}}^{\mathrm{odd}}$) shown in Fig. 5 agree well with (8) and (14). The frequency responses with various values of k_2 are exhibited in Fig. 6. It can be observed from Fig. 6*a* that constant in-band return losses level and various passband BWs are obtained with various values of k_2 under even-mode excitation. As shown in Fig. 6*b*, under odd-mode excitation, constant passband BW and various in-band return losses could be realised with various values of k_2. Accordingly, under odd-mode excitation, the passband BW can be adjusted by tuning the value of k_1. Under even-mode excitation, the passband BW can be changed by tuning the value of k_2.

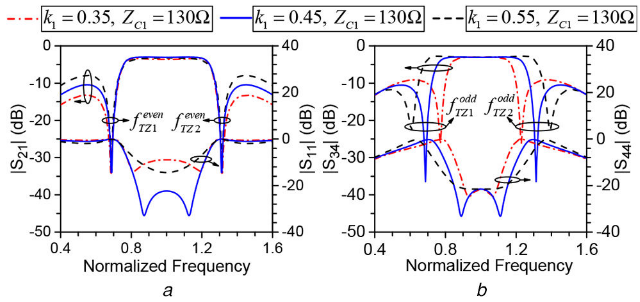

Fig. 5 *Normalised frequency responses with various k_1*
(a) S_{21} and S_{11}, ***(b)*** S_{34} and S_{44} ($Z_1 = 65\,\Omega$, $Z_{2a} = 145\,\Omega$, and $Z_{2b} = 65\,\Omega$)

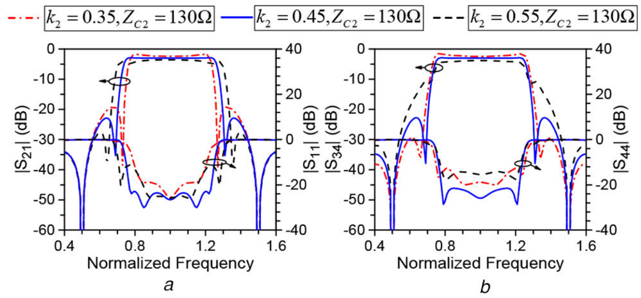

Fig. 6 *Normalised frequency responses with various k_2*
(a) S_{21} and S_{11}, ***(b)*** S_{34} and S_{44} ($Z_1 = 65\,\Omega$, $Z_{1a} = 145\,\Omega$, and $Z_{1b} = 65\,\Omega$)

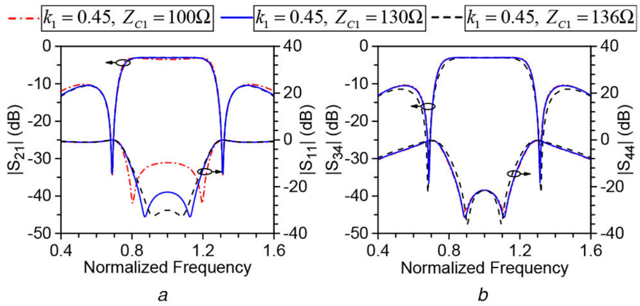

Fig. 7 *Normalised frequency responses with various Z_{C1}*
(a) S_{21} and S_{11}, ***(b)*** S_{34} and S_{44} ($Z_1 = 65\,\Omega$, $Z_{2a} = 145\,\Omega$, and $Z_{2b} = 65\,\Omega$)

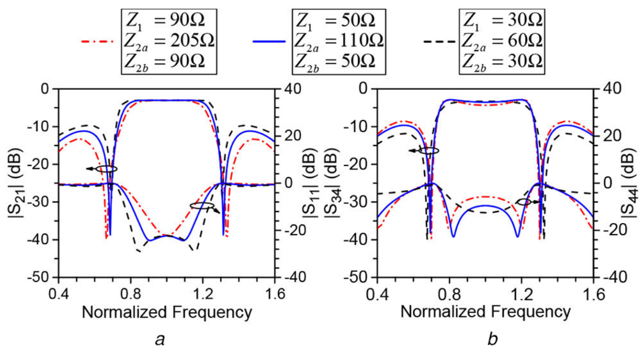

Fig. 8 *Normalised frequency responses with various Z_1, while Z_{2a} and Z_{2b} are chosen to achieve equal power splitting across the passband range*
(a) S_{21} and S_{11}, ***(b)*** S_{34} and S_{44} ($k_1 = 0.45$ and $Z_{C1} = 130\,\Omega$)

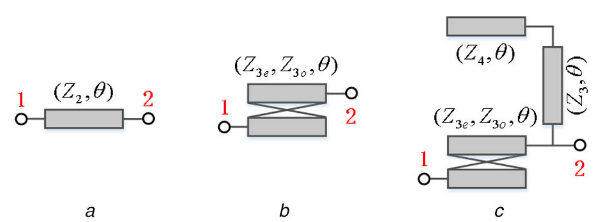

Fig. 9 *Three different kinds of IT structures*

As depicted in Fig. 7*a*, when changing the value of Z_{c1}, constant passband BW and various in-band return losses can be observed under even-mode excitation. Thus, S_{11} can be optimised by tuning the value of Z_{c1}, which accords to (7b). It can be observed from Fig. 7*b* that S_{44} almost maintain constant with various values of Z_{c1}, which has a good agreement with (13b).

Fig. 8 shows the normalised frequency responses with various values of Z_1 (Z_{2b} is chosen to be equal to Z_1), and Z_{2a} is adjusted to achieve equal power splitting across the passband range. As observed in Fig. 8*a*, under even-mode excitation, various passband BWs and constant in-band return loss could be observed in the in-phase operation by tuning the value of Z_1. It can be seen from Fig. 8*b* that constant passband BW and various in-band return losses are realised in the out-of-phase operation by changing the value of Z_1, which accords to (13b). Consequently, the passband BW of S_{21} and S_{34} can be adjusted by tuning the values of k_2 and k_1, while the in-band return loss level of S_{11} and S_{44} can be optimised by changing the values of Z_{C1} and Z_1, respectively.

4 Operating principles of FRWC

4.1 Analysis of proposed FRWC (type B)

The FRWC could be obtained by loading IT structures into FRCC. According to a simplified even-mode equivalent circuit shown in Fig. 3*c*, the ***ABCD*** matrix between port 1 and port 2 can be deduced as (15). Moreover, the matrix between port 4 and port 2 can be deduced as (16) based on the simplified odd-mode equivalent circuit shown in Fig. 3*d*

$$\begin{pmatrix} \boldsymbol{A}_{12} & \boldsymbol{B}_{12} \\ \boldsymbol{C}_{12} & \boldsymbol{D}_{12} \end{pmatrix} = \begin{pmatrix} \boldsymbol{A}_{\mathrm{IT1}} & \boldsymbol{B}_{\mathrm{IT1}} \\ \boldsymbol{C}_{\mathrm{IT1}} & \boldsymbol{D}_{\mathrm{IT1}} \end{pmatrix}^{-1} \begin{pmatrix} \boldsymbol{A}_{N1} & \boldsymbol{B}_{N1}/2 \\ 2\boldsymbol{C}_{N1} & \boldsymbol{D}_{N1} \end{pmatrix} \tag{15}$$

where

$$\begin{pmatrix} \boldsymbol{A}_{N1} & \boldsymbol{B}_{N1} \\ \boldsymbol{C}_{N1} & \boldsymbol{D}_{N1} \end{pmatrix} = \begin{pmatrix} \boldsymbol{A}_{\mathrm{TCL1}} & \boldsymbol{B}_{\mathrm{TCL1}} \\ \boldsymbol{C}_{\mathrm{TCL1}} & \boldsymbol{D}_{\mathrm{TCL1}} \end{pmatrix} \begin{pmatrix} \boldsymbol{A}_{\mathrm{IT2}} & \boldsymbol{B}_{\mathrm{IT2}} \\ \boldsymbol{C}_{\mathrm{IT2}} & \boldsymbol{D}_{\mathrm{IT2}} \end{pmatrix}$$

$$\begin{pmatrix} \boldsymbol{A}_{42} & \boldsymbol{B}_{42} \\ \boldsymbol{C}_{42} & \boldsymbol{D}_{42} \end{pmatrix} = \begin{pmatrix} \boldsymbol{A}_{\mathrm{IT3}} & \boldsymbol{B}_{\mathrm{IT3}} \\ \boldsymbol{C}_{\mathrm{IT3}} & \boldsymbol{D}_{\mathrm{IT3}} \end{pmatrix}^{-1} \begin{pmatrix} \boldsymbol{A}_{N2} & \boldsymbol{B}_{N2}/2 \\ 2\boldsymbol{C}_{N2} & \boldsymbol{D}_{N2} \end{pmatrix} \tag{16}$$

where

$$\begin{pmatrix} \boldsymbol{A}_{N2} & \boldsymbol{B}_{N2} \\ \boldsymbol{C}_{N2} & \boldsymbol{D}_{N2} \end{pmatrix} = \begin{pmatrix} \boldsymbol{A}_{\mathrm{TCL2}} & \boldsymbol{B}_{\mathrm{TCL2}} \\ \boldsymbol{C}_{\mathrm{TCL2}} & \boldsymbol{D}_{\mathrm{TCL2}} \end{pmatrix} \begin{pmatrix} \boldsymbol{A}_{\mathrm{IT2}} & \boldsymbol{B}_{\mathrm{IT2}} \\ \boldsymbol{C}_{\mathrm{IT2}} & \boldsymbol{D}_{\mathrm{IT2}} \end{pmatrix}$$

In this study, three different kinds of IT structures shown in Fig. 9 are employed to construct the proposed FRWC. Define $X_{T3} = Z_3\cot\theta(\tan^2\theta - R_Z)/(1 + R_Z)$ and $R_Z = Z_4/Z_3$, and the ***ABCD*** matrices of IT structures exhibited in Fig. 9 can be expressed as (17)–(19). By substituting (17)–(19) into (15) and (16), the transmission characteristics of the proposed FRWC could be obtained, theoretically

$$\begin{pmatrix} \boldsymbol{A}_{\mathrm{ITa}} & \boldsymbol{B}_{\mathrm{ITa}} \\ \boldsymbol{C}_{\mathrm{ITa}} & \boldsymbol{D}_{\mathrm{ITa}} \end{pmatrix} = \begin{pmatrix} \cos\theta & \mathrm{j}Z_2\sin\theta \\ \dfrac{\mathrm{j}\sin\theta}{Z_2} & \cos\theta \end{pmatrix} \tag{17}$$

$$\begin{pmatrix} \boldsymbol{A}_{\mathrm{ITb}} & \boldsymbol{B}_{\mathrm{ITb}} \\ \boldsymbol{C}_{\mathrm{ITb}} & \boldsymbol{D}_{\mathrm{ITb}} \end{pmatrix} = \begin{pmatrix} \dfrac{Z_{3a}}{Z_{3b}}\cos\theta & \dfrac{Z_{3a}^2\cot^2\theta - \mathrm{j}Z_{3b}^2\csc^2\theta}{Z_{3b}\csc\theta} \\ \mathrm{j}\dfrac{1}{Z_{3b}\csc\theta} & -\dfrac{Z_{3a}}{Z_{3b}}\cos\theta \end{pmatrix} \tag{18}$$

Based on our previous work [19], the frequencies of TZs produced by ITc structures could be deduced as

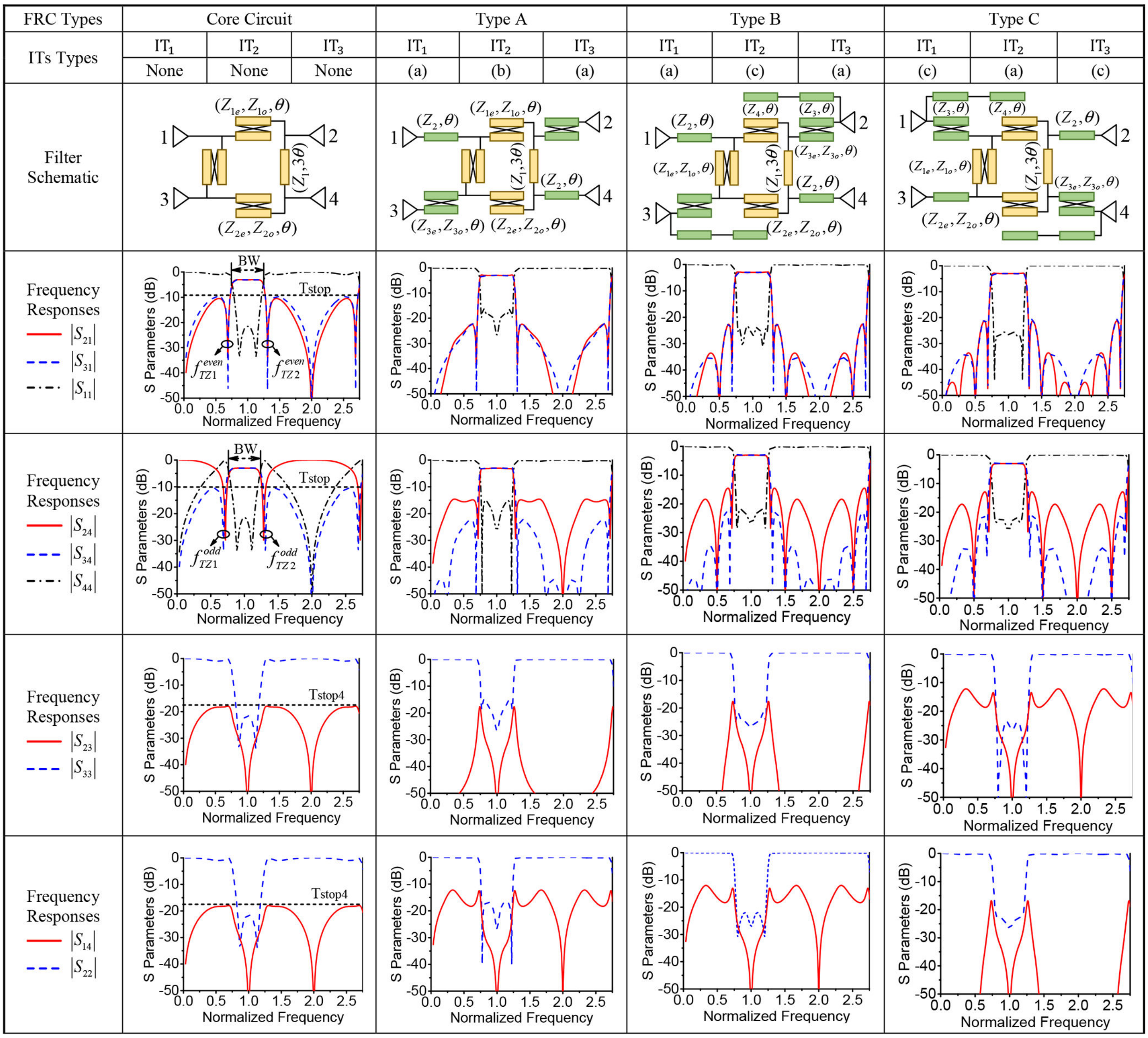

Fig. 10 *Frequency responses of four FRC with varied ITs*

$$\begin{pmatrix} \boldsymbol{A}_{\mathrm{ITc}} & \boldsymbol{B}_{\mathrm{ITc}} \\ \boldsymbol{C}_{\mathrm{ITc}} & \boldsymbol{D}_{\mathrm{ITc}} \end{pmatrix} = \begin{pmatrix} \dfrac{Z_{3a}}{Z_{3b}}\cos\theta + \dfrac{Z_{3b}^2\csc^2\theta - Z_{3a}^2\cot^2\theta}{X_{T3}Z_{3b}\csc\theta} & \mathrm{j}\dfrac{Z_{3b}^2\csc^2\theta - Z_{3a}^2\cot^2\theta}{Z_{3b}\csc\theta} \\ \mathrm{j}\dfrac{1}{Z_{3b}\csc\theta} - \mathrm{j}\dfrac{Z_{3a}}{X_{T3}Z_{3b}}\cos\theta & \dfrac{Z_{3a}}{Z_{3b}}\cos\theta \end{pmatrix} \tag{19}$$

$$f_{\mathrm{TZ}1}^{\mathrm{ITc}} = \frac{2f_0}{\pi}\arctan\sqrt{R_Z} \tag{20a}$$

$$f_{\mathrm{TZ}2}^{\mathrm{ITc}} = 2f_0 - \frac{2f_0}{\pi}\arctan\sqrt{R_Z} \tag{20b}$$

Under even-mode excitation of FRWC (type B), the expression of S_{11} at centre frequency (f_0) can be simplified as (21) based on (15) and TL theory

$$S_{11} = \left|\frac{2\cdot Z_2^2\cdot Z_{3b}^2 - Z_0^2\cdot Z_{1b}^2}{2\cdot Z_2^2\cdot Z_{3b}^2 + Z_0^2\cdot Z_{1b}^2}\right| \tag{21}$$

According to (16), the expression of S_{44} at f_0 under odd-mode excitation can be simplified as

$$S_{44} = \left|\frac{2\cdot Z_2^2\cdot Z_{3b}^2 - Z_0^2\cdot Z_1^2}{2\cdot Z_2^2\cdot Z_{3b}^2 + Z_0^2\cdot Z_1^2}\right| \tag{22}$$

The proposed FRCC prototype and FRWC adopting various kinds of IT structures are shown in Fig. 10. Specifically, Fig. 10 and Table 1 show the schematics, frequency responses, passband BW, circuit size as well as specific design parameters. Moreover, the initial design parameters can be obtained based on (7b), (13b), (21), and (22). In FRWC (type B), the coupled lines ((Z_{1e}, Z_{1o}, θ), (Z_{2e}, Z_{2o}, θ)) are adopted in the designed rat-race coupler to realise a wide passband BW, and coupled lines (Z_{3e}, Z_{3o}, θ) connected with open-circuited stubs ((Z_3, θ), (Z_4, θ)) are employed to obtain better impedance matching and deeper out-of-band rejection. According to our previous study [19], the coupled lines structure can provide broadband impedance transformation and good filtering characteristics. Therefore, we use the CLs to replace the TL, then obtain broad operating BW, as observed in Fig. 10.

The simulated phase imbalances results of the conventional coupler exhibited in Fig. 1*a* and presented coupler (type B) are shown in Fig. 11. Accordingly, the simulated phase imbalances BWs with the level <±7° are 0.7 and 1.34 GHz in the conventional

Table 1 Operating characteristics of four FRC with varied ITs

FRC types	Core circuit				Type A				Type B				Type C			
FBW, %	51				52				53.5				53.5			
circuit size	$0.25\lambda_g \times 0.25\lambda_g$				$0.75\lambda_g \times 0.25_g$				$0.75\lambda_g \times 0.35\lambda_g$				$0.75\lambda_g \times 0.35\lambda_g$			
number of TZs (≤$2f_0$)	$\|S_{21}\|$	$\|S_{31}\|$	$\|S_{42}\|$	$\|S_{43}\|$	$\|S_{21}\|$	$\|S_{31}\|$	$\|S_{42}\|$	$\|S_{43}\|$	$\|S_{21}\|$	$\|S_{31}\|$	$\|S_{42}\|$	$\|S_{43}\|$	$\|S_{21}\|$	$\|S_{31}\|$	$\|S_{42}\|$	$\|S_{43}\|$
	4	4	4	4	4	4	4	6	6	6	6	8	8	6	6	6
number of TPs in passband	$\|S_{11}\|$	$\|S_{22}\|$	$\|S_{33}\|$	$\|S_{44}\|$	$\|S_{11}\|$	$\|S_{22}\|$	$\|S_{33}\|$	$\|S_{44}\|$	$\|S_{11}\|$	$\|S_{22}\|$	$\|S_{33}\|$	$\|S_{44}\|$	$\|S_{11}\|$	$\|S_{22}\|$	$\|S_{33}\|$	$\|S_{44}\|$
	2	2	2	2	3	3	3	3	3	3	3	3	3	3	3	3
performance (in passband)	$S_{11} < -16.5$ dB, $S_{22} < -14.1$ dB $S_{33} < -12.1$ dB, $S_{44} < -10.4$ dB $S_{14} < -18.5$ dB, $S_{23} < -18.5$ dB				$S_{11} < -16.2$ dB, $S_{22} < -16.8$ dB, $S_{33} < -15.0$ dB, $S_{44} < -15.0$ dB, $S_{14} < -20.0$ dB, $S_{23} < -20.0$ dB				$S_{11} < -22.5$ dB, $S_{22} < -25.5$ dB, $S_{33} < -21.9$ dB, $S_{44} < -23.8$ dB, $S_{14} < -21.5$ dB, $S_{23} < -20.0$ dB				$S_{11} < -25.5$ dB, $S_{22} < -22.5$ dB, $S_{33} < -23.6$ dB, $S_{44} < -21.8$ dB, $S_{14} < -23.5$ dB, $S_{23} < -23.5$ dB			
IT characteristic	no				yes				yes				yes			
design parameters	$Z_{1e} = 210\ \Omega$, $Z_{1o} = 80\ \Omega$, $Z_{2e} = 210\ \Omega$, $Z_{2o} = 80\ \Omega$, $Z_1 = 65\ \Omega$				$Z_{1e} = 210\ \Omega$, $Z_{1o} = 80\ \Omega$, $Z_{2e} = 210\ \Omega$, $Z_{2o} = 80\ \Omega$, $Z_{3e} = 210\ \Omega$, $Z_{3o} = 108\ \Omega$, $Z_1 = 65\ \Omega$, $Z_2 = 43\ \Omega$				$Z_{1e} = 210\ \Omega$, $Z_{1o} = 80\ \Omega$, $Z_{2e} = 210\ \Omega$, $Z_{2o} = 80\ \Omega$, $Z_{3e} = 222\ \Omega$, $Z_{3o} = 120\ \Omega$, $Z_1 = 65\ \Omega$, $Z_2 = 43\ \Omega$, $Z_3 = 120\ \Omega$, $Z_4 = 120\ \Omega$				$Z_{1e} = 210\ \Omega$, $Z_{1o} = 80\ \Omega$, $Z_{2e} = 210\ \Omega$, $Z_{2o} = 80\ \Omega$, $Z_{3e} = 210\ \Omega$, $Z_{3o} = 108\ \Omega$, $Z_1 = 65\ \Omega$, $Z_2 = 43\ \Omega$, $Z_3 = 120\ \Omega$, $Z_4 = 120\ \Omega$			

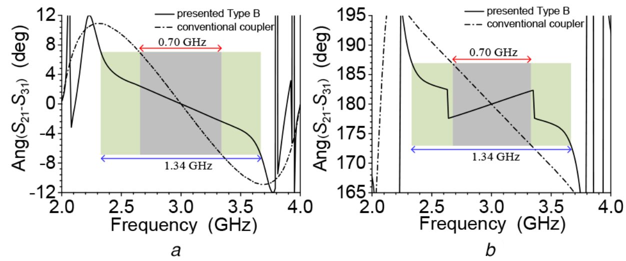

Fig. 11 *Simulated phase imbalance results of conventional coupler and presented coupler*
(a) In-phase operation, *(b)* Out-of-phase operation

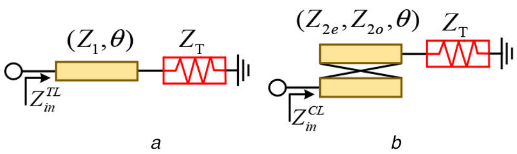

Fig. 12 *Schematics of specific*
(a) TL, *(b)* CLs

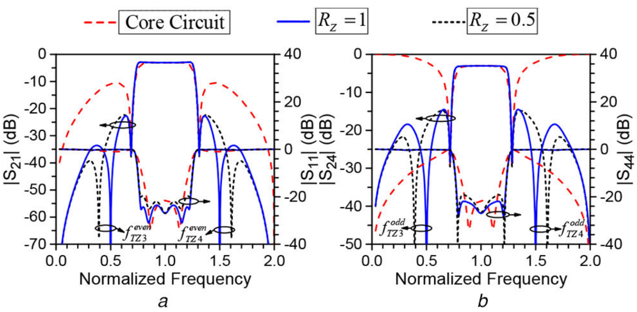

Fig. 13 *Normalised frequency responses of FRCC and FRWC (type B) with various* R_Z
(a) S_{21} and S_{11}, *(b)* S_{34} and S_{44} ($k_1 = 0.45$, $Z_{C1} = 130\,\Omega$, $Z_1 = 65\,\Omega$, $Z_{2a} = 145\,\Omega$, and $Z_{2b} = 65\,\Omega$)

coupler and designed coupler, respectively. Compared with the conventional coupler, the phase imbalances in the designed coupler are improved greatly.

The CLs shown in Fig. 12*b* can be simplified as TL exhibited in Fig. 12*a* at f_0. However, the transmission characteristic in TL and CLs are not exactly equal during operating frequencies. The presented rat-race coupler structure (type B) is asymmetric during passband. Thus, the phase imbalance in the designed rat-race coupler is larger than other works [2–5]. Some methods are proposed to improve phase imbalance. Two extra short-circuited

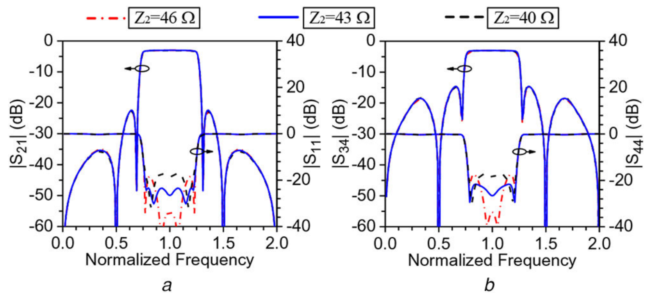

Fig. 14 *Normalised frequency responses with various* Z_2
(a) S_{21} and S_{11}, *(b)* S_{34} and S_{44} ($k_1 = 0.45$, $Z_{C1} = 130\,\Omega$, $R_Z = 1$, $Z_{2a} = 145\,\Omega$, and $Z_{2b} = 65\,\Omega$)

stubs with the characteristic impedance equal to the even-mode impedance of the coupled-line section are adopted in [2] to make the equivalent circuit fully symmetric, resulting in good phase imbalance. Multi-sectional branch-line couplers [3, 4] and coupler composed of slow-wave structure [5] are introduced to realise good phase imbalances.

The operating mechanism, theoretical analysis, and design procedure of FRWC (type B) are discussed in the following. The operating mechanisms of FRCC and FRWC (type A) are similar to the working mechanisms of FRWC (type A).

To explain the influences of IT structures, the frequency responses of FRCC and FRWC (type B) are shown in Fig. 13. Extra TZs could be introduced in the in-phase operation (f_{TZ3}^{even}, f_{TZ4}^{even}) and out-of-phase operation (f_{TZ3}^{odd}, f_{TZ4}^{odd}) by employing ITc structure. As observed in Fig. 9, the frequencies of TZs (f_{TZ3}^{even}, f_{TZ4}^{even}, f_{TZ3}^{odd}, and f_{TZ4}^{odd}) could be adjusted by tuning the value of R_Z, which agrees well with (20). According to Fig. 14, in FRWC (type B), constant passband BW and various in-band return losses can be realised in the in-phase operation and out-of-phase operation by tuning the value of Z_2.

To further analyse impedance matching performance of FRWC (type B), normalised frequency responses of FRWC (type B) with different characteristic impedance in input and output ports are exhibited in Fig. 15. As observed in Fig. 15, S_{11} and S_{44} of the designed FRWC (type B) with the level better than 11.5 dB can be obtained when the characteristic impedances in ports 1, 2, 3, and 4 are selected from 35 to 90 Ω, and the detailed values of Z_{3e}, Z_{3o} and Z_2 are exhibited in Table 2. Thus, the impedance matching performance of FRWC (type B) can be optimised by tuning the detailed values of IT structures.

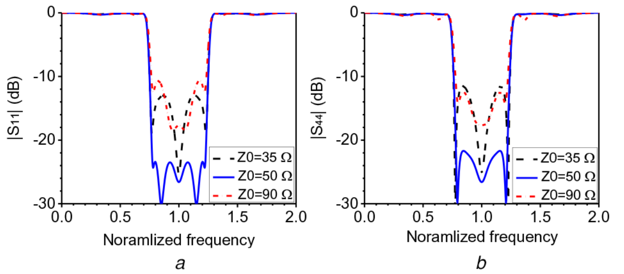

Fig. 15 *IT characteristics of FRC when characteristic impedance of ports 1, 2, 3 and 4 are selected as 35, 50, and 90 Ω*

Table 2 Design parameters of three cases with various impedance matching performance

	Z_{3e}, Ω	Z_{3o}, Ω	Z_2, Ω
case 1 ($Z_0 = 35$ Ω)	220	120	39
case 2 ($Z_0 = 50$ Ω)	220	120	43
case 3 ($Z_0 = 90$ Ω)	200	83	62

4.2 Design procedures of proposed FRWC (type B)

According to the above analysis, the practical design procedure of the proposed FRWC is summarised as follows:

(i) Determine the desired f_0, BW_{21}, BW_{24}, passband selectivity performance, stopband rejection level, and characteristic impedances in ports 1, 2, 3, and 4.
(ii) Design FRCC and obtain the initial parameter values of Z_1, Z_{1e}, Z_{1o}, Z_{2e}, and Z_{2o} based on 7(b) and 13(b).
(iii) According to Figs. 5 and 6, the required BW_{21} and BW_{24} can be realised by changing the values of k_2 and k_1, respectively.
(iv) Meeting $Z_{2b} = Z_1$, change Z_{2a} to achieve equally splitting across the passband range, following Fig. 4. Also, the arbitrary power splitting ratio can be realised according to Fig. 4.
(v) Optimise the in-band return loss in port 1 (port 4) by adjusting Z_{c1} (Z_1), respectively, according to Figs. 7 and 8.
(vi) Add corresponding IT structures into FRCC and the initial values of Z_{3e}, Z_{3o}, and Z_2 can be calculated from (21) and (22).
(vii) Adjust the value of Z_2 to obtain good impedance in ports 1 and 4, impedance matching in ports 2 and 3 could be optimised by tuning the value of Z_{3e} and Z_{3o}.
(viii) Return to step (iii) for further optimisation until the desired performances are achieved.

Owing to the inhomogeneous dielectric material in the microstrip line, the even- and odd-mode propagation velocities for microstrip coupled lines are not equal and the differences between them become frequency-dependent, which will lead to a shift of TZs [20–22]. A stripline structure is one solution for the coupled lines to have identical even- and odd-mode propagation constants. However, the stripline is difficult to implement and complex for fabrication, especially when via-hole groundings are used.

To explain the effect of mode phase velocities of the coupled-line section on the performance of the proposed rat-race coupler, Fig. 16 shows the circuit-simulated magnitude responses for the presented rat-race coupler using microstrip coupled lines ($\theta_e = 91.5°$ and $\theta_o = 88.5°$ at f_0) and stripline coupled lines ($\theta_e = \theta_o = 90°$ at f_0). As observed in Fig. 16, compared with the presented rat-race coupler employing stripline CLs, the TZ around $2f_0$ (6 GHz) in the rat-race coupler utilising microstrip CLs shifts to a higher frequency, and the stopband rejection performances are reduced.

5 Experimental verification

To validate the above theoretical analysis, a wideband FRC based on FRWC (type B) structure was designed and fabricated on the substrate with a dielectric constant of 2.55 and a thickness of 31

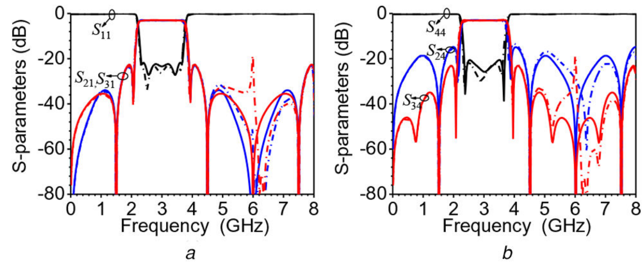

Fig. 16 *Magnitude responses of presented rat-race coupler employing stripline (solid lines, $\theta_e = \theta_o$ at f_o) and microstrip coupled lines (dash lines, $\theta_e \neq \theta_o$ at f_o)*

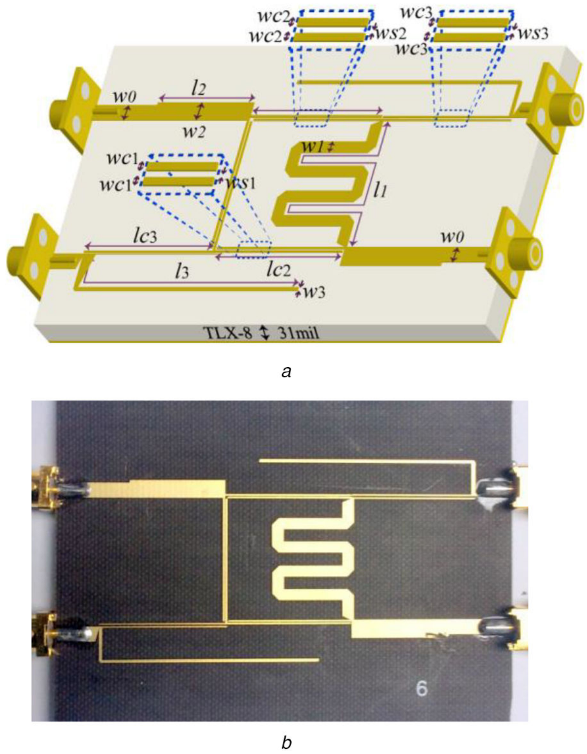

Fig. 17 *The layout and photo of FRWC (type B)*
(a) Layout of designed FRWC (type B) (w1 = 1.4 mm, l1 = 52.1 mm, w2 = 2.7 mm, l2 = 17.1 mm, w3 = 0.38 mm, l3 = 17.9 mm, wc1 = wc2 = 0.2 mm, ws1 = ws2 = 0.16 mm, lc1 = lc2 = 18.4 mm, wc3 = 0.15 mm, ws3 = 0.35 mm, lc3 = 18.3 mm), ***(b)*** Photo of FRWC (type B)

mil. The circuit layout and photograph are shown in Figs. 17*a* and *b*, respectively.

Firstly, the fabricated circuit was measured as a filtering power divider. The electromagnetic (EM)-simulated and measured results of the in-phase operation are depicted in Fig. 18. According to Fig. 18*a*, the measured passband is wider than the EM-simulated one, it is due to slight over-coupling in coupled TLs. The measured centre frequency is located at 3.16 GHz and the FBW is 48.1% with the return loss better than 10 dB. Within the passband, the minimum insertion losses of S_{21} and S_{31} are $3 + 1.07$and $3 + 1.04$ dB, respectively. The stopband extends to $2.53f_0$ with more than 20 dB rejection level. As shown in Fig. 18*b*, the measured amplitude differences between S_{21} and S_{31} is <±0.3 dB ranging from 2.37 to 3.76 GHz, while measured phase differences of $|S_{21}| - |S_{31}|$ is $< \pm 7°$ during 2.57–3.67 GHz. As shown in Fig. 18*c*, the output return loss (S_{33}) is better than 18.5 dB ranging from 2.5 to 3.7 GHz, and the isolation performance between port 2 and port 3 is better than 20 dB from DC to 8.0 GHz.

Then, the fabricated circuit was measured as a filtering balun to verify the performance of out-of-phase operation. Fig. 19 shows the EM-simulated and measured results of out-of-phase operation. As shown in Fig. 19*a*, the measured S_{44} is better than 10 dB ranging from 2.37 to 3.8 GHz. The measured minimum magnitude of S_{24}

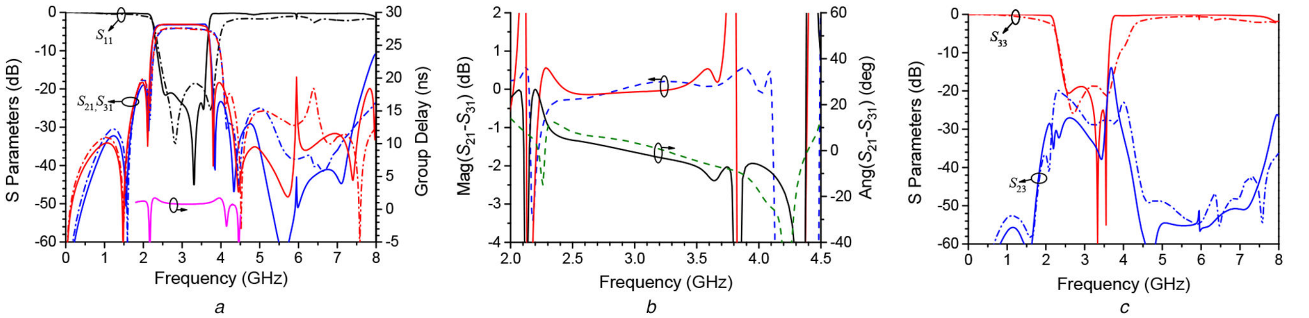

Fig. 18 *EM-simulated and measured results of in-phase operation (solid lines represent EM simulation results and dotted lines represent measured results)*
(a) Transmission characteristics, ***(b)*** Amplitude and phase imbalances, ***(c)*** Isolation characteristics

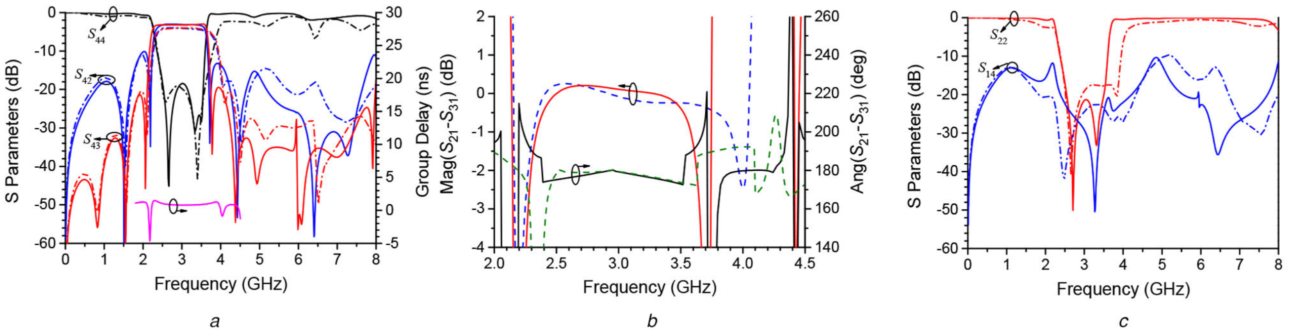

Fig. 19 *EM-simulated and measured results of out-of-phase operation (solid lines represent EM simulation results and dotted lines represent measured results)*
(a) Transmission characteristic, ***(b)*** Amplitude and phase imbalances, ***(c)*** Isolation characteristics

Table 3 Comparisons between the proposed rat-race coupler and published similar designs

	f_0, GHz	FBW	Insertion loss, dB	Filtering response	Amplitude imbalance, dB	Phase imbalance, deg	S21 stopband, dB	S43 stopband, dB	Effective size ($\lambda_g \times \lambda_g$)
[3]	1.5	70.2%	3.4	N	0.37	±0.5	—	—	0.31 × 0.34
[5]	2.3	34.2%	—	N	1.45	±2	—	—	0.73 × 0.73
[6]	2.0	100%	3.35	N	1	±10	—	—	0.75 × 0.75
[12]	2.0	5.0%	4.4	Y	—	±0.9	$4.3f_0$ (<30 dB)	$4.3f_0$ (<30 dB)	0.153 × 0.195
[14]	1.5	4.0	6	Y	—	−8/12	$2.73f_0$ (<50 dB)	—	0.31 × 0.22
[15]	0.47	13%	4.17	Y	0.1	±4.5	$5f_0$ (<20 dB)	$5f_0$ (<20 dB)	0.095 × 0.117
[16]	2.33	4.94%	4.77	Y	—	±0.9	$2.33f_0$ (<25 dB)	$2.33f_0$ (<20 dB)	0.196 × 0.212
this work	3.08	35.2%	3.95	Y	0.3	±7	$2.53f_0$ (<20 dB)	$2.53f_0$ (<20 dB)	0.75 × 0.35

and S_{34} is 3 + 0.95 and 3 + 1.01 dB in the passband. The out-of-band rejection of S_{24} extends to $2.53f_0$ with rejection level better than 17 dB, and the stopband of S_{34} extends to $2.53f_0$ with rejection level better than 20 dB. According to Fig. 19*b*, the measured amplitude differences between S_{24} and S_{34} is <±0.3 dB ranging from 2.35 to 3.65 GHz, while measured phases differences between S_{24} and S_{34} is ranging from 174° to 180° during 2.37–3.48 GHz. As shown in Fig. 19*c*, the output return loss (S_{22}) is better than 17.2 dB.

Table 3 summarises the performances of our proposed rat-race coupler and similar designs. The presented rat-race coupler realises the widest BW among the published FRCs.

6 Conclusion

In this study, a novel rat-race coupler with various kinds of IT structures is proposed. Based on the proposed structure, the fabricated rat-race coupler with a FBW of 35.2% could realise high selectivity and deep stopband rejection performances both in the in-phase operation and out-of-phase operation. The design formulas have been derived and verified. Moreover, a detailed design procedure has been demonstrated, which is helpful for its practical application.

7 Acknowledgment

This work was supported in part by the National Natural Science Foundations of China (nos. 61701041, 61671084, and 61821001), the Bupt Excellent Ph.D. Students Foundation (no. CX2019302), and the China Scholarship Council.

8 References

[1] Chang, C.Y., Yang, C.C.: 'A novel broad-band Chebyshev-response rat-race ring coupler', *IEEE Trans. Microw. Theory Tech.*, 1999, **47**, (4), pp. 455–462

[2] Chang, W.S., Liang, C.H., Chang, C.Y.: 'Wideband high-isolation and perfect-balance microstrip rat-race coupler', *Electron. Lett.*, 2012, **48**, (7), pp. 382–384

[3] Tang, C.W., Tseng, C.T., Hsu, K.C.: 'Design of wide passband microstrip branch-line couplers with multiple sections', *IEEE Trans. Compon. Packag. Manuf. Technol.*, 2014, **4**, (7), pp. 1222–1227

[4] Li, E.S., Kang, C.J.: 'Properties of multisection transdirectional coupled-line couplers', *IET Microw. Antennas Propag.*, 2018, **12**, (7), pp. 1166–1174

[5] Kurgan, P., Koziel, S.: 'Design of high-performance hybrid branch-line couplers for wideband and space-limited applications', *IET Microw. Antennas Propag.*, 2016, **10**, (12), pp. 1339–1344

[6] Chou, P.J., Lin, Y.W., Chang, C.Y.: 'Exact synthesis of full- and half-symmetric rat-race ring hybrids with or without impedance transforming characteristics', *IEEE Trans. Microw. Theory Tech.*, 2015, **63**, (12), pp. 3971–3980

[7] Gao, L., Qamar, Z., Zhang, H.L., *et al.*: 'Wideband arbitrary phase-difference coupled-line coupler with tight coupling coefficient and small phase variation', *IET Microw. Antennas Propag.*, 2018, **12**, (15), pp. 2356–2363

[8] Jiao, L., Wu, Y., Liu, Y., *et al.*: 'Concept of narrow-band filtering rat-race cross-shaped dielectric', *Electron. Lett.*, 2016, **52**, (3), pp. 212–213

[9] Cheng, Y. J., Fan, Y.: 'Compact substrate-integrated waveguide bandpass rat-race coupler and its microwave applications', *IET Microw. Antennas Propag.*, 2012, **6**, (9), pp. 1000–1006

[10] Liu, W.R., Huang, T.Y., Chen, C.F., *et al.*: 'Design of a 180-degree hybrid with Chebyshev filtering response using coupled resonators'. 2013 IEEE MTT-S Int. Microwave Symp. Digest, Seattle, WA, USA, 2013, pp. 1–3

[11] Lin, C.K., Chung, S.J.: 'A compact filtering 180° hybrid', *IEEE Trans. Microw. Theory Tech.*, 2011, **59**, (12), pp. 3030–3036

[12] Wang, K.X., Liu, X.F., Li, Y.C., *et al.*: 'LTCC filtering rat-race coupler based on eight-line spatially-symmetrical coupled structure', *IEEE Access*, 2017, **6**, pp. 262–269

[13] Wang, W.H., Shen, T.M., Huang, T.Y., *et al.*: 'Miniaturized rat-race coupler with bandpass response and good stopband rejection'. 2009 IEEE MTT-S Int. Microwave Symp. Digest, Boston, MA, USA, 2009, pp. 709–712

[14] Chen, C.F., Huang, T.Y., Chen, C.C., *et al.*: 'A compact filtering rat-race coupler using dual-mode stub-loaded resonators'. 2012 IEEE MTT-S Int. Microwave Symp. Digest, Montreal, Canada, 2012, pp. 1–3

[15] Wang, K.X., Zhang, X.Y., Zheng, S.Y., *et al.*: 'Compact filtering rat-race hybrid with wide stopband', *IEEE Trans. Microw. Theory Tech.*, 2015, **63**, (8), pp. 2550–2560

[16] Lin, T.W., Wu, J.Y., Kuo, J.T.: 'Filtering rat-race coupler with transmission zeros using compact miniaturized hairpin resonators'. 2015 IEEE MTT-S Int. Microwave Symp. Digest, Shenzhen, China, 2015, pp. 1–4

[17] Ang, K.S., Leong, Y.C.: 'Converting baluns into broad-band impedance-transforming 180° hybrids', *IEEE Trans. Microw. Theory Tech.*, 2002, **50**, (8), pp. 1990–1995

[18] Tang, C.W., Tseng, C.T., Wu, P.H.: 'Design of wide passband/stopband microstrip bandpass filters with the stepped coupled line', *IEEE Trans. Microw. Theory Tech.*, 2013, **61**, (3), pp. 1095–1103

[19] Zhang, B., Yu, C.P., Liu, Y.A. 'Compact power divider with bandpass response and improved out-of-band rejection', *J. Electromagn. Wave Appl.*, 2016, **30**, (9), pp. 1124–1132

[20] Shaman, H., Hong, J.-S.: 'Input and output cross-coupled wideband bandpass filter', *IEEE Trans. Microw. Theory Tech.*, 2007, **55**, (12), pp. 2562–2568

[21] Xu, K.-D., Li, D.-H., Liu, Y.-H.: 'High-selectivity wideband bandpass filter using simple coupled lines with multiple transmission Poles and zeros', *IEEE Microw. Wirel. Compon. Lett.*, 2019, **29**, (2), pp. 107–109

[22] Xu, K.-D., Zhang, F.-Y., Liu, Y.-H., *et al.*: 'Bandpass filter using three pairs of coupled lines with multiple transmission zeros', *IEEE Microw. Wirel. Compon. Lett.*, 2019, **28**, (7), pp. 576–578